LUND UNIVERSITY
Faculty of Science
Division of Nuclear physics

MAGNETIC FIELD DESIGN FOR POLARISED NEUTRONS IN EUROPEAN SPALLATION NEUTRON SOURCE INSTRUMENTS

Bachelor thesis by : Andrea Monzani

Supervised by : Wai Tung Lee
Co-supervised by : Joakim Cederkall

May 2021

Abstract

The goal of this project is the design of the magnetic field of the neutron analyser for the European Spallation Source instrument DREAM (Diffraction Resolved by Energy and Angle Measurements). This instrument is a neutron diffractometer and its purpose is the determination of the magnetic and chemical structure of materials. Simulations have been performed over the span of a semester using the Finite Element Method (FEM) in a software called COMSOL Multiphysics. Three different setups, with different guide fields, have been investigated and compared in order to achieve the best results. This has required to study how to produce highly uniform magnetic fields with coils. The initial setup, where the guide was composed by four rectangular coils, was found not to meet the required field characteristics concerning adiabaticity and uniformity. The second setup, which comprised also four compensation coils, fulfilled the specifications. However, a third setup based on a Halbach four-coil exceeded the required field characteristics and thus allows for potential imperfections in the manufacturing of the coils. As part of this work, different aspects of neutron physics have been investigated, including, neutron scattering, spin-filtering and spin-transport, which are the main physics principles behind DREAM.

Contents

1 Introduction

1.1 Aim of the study

The main purpose of this work is the design of the magnetic field of the polarisation analyser and of the guide field in the ESS diffractometer DREAM. In this process, different aspects of neutron physics are investigated, e.g., neutron scattering, spin filtering and spin-transport. In particular, the magnetic field has to be designed so that the neutron spin-transport and spin-filtering are optimized. The computations are done with the help of a numerical method called Finite Element (FEM) which is implemented in a simulation software called COMSOL Multiphysics [1]. These concepts and the results of the study are explained in the following sections.

1.2 Physics background and motivation

Neutron scattering, similarly to X-ray scattering, is a very efficient technique to gain information about the structure of a sample. Neutron and X-ray scattering are complementary techniques. Their similarity being:

1. Both can be used to identify the location of atoms or ions and magnetic moments.
2. The wavelength range in both techniques can be selected to match the length-scale suitable for condensed matter studies, typically in the nanometer range.

The main difference that makes them complementary techniques arises from the nature of the interaction that gives rise to scattering. Neutron scattering comes from both the strong-force interaction between the neutron and the atomic nuclei and the magnetic interaction between the neutron spin and the magnetic field produced by the atomic or ionic magnetic moments. X-ray scattering arises from electromagnetic interaction between the atomic electrons with X-rays. The consequences are the following:

1. Neutron-nucleus scattering identifies where the nuclei are and therefore where the atoms or ions are. The scattering is independent of the electronic structure. X-ray scattering on the other hand probes the electronic structure, but it also makes it more complicated to analyse and obtain the positions of the atoms or ions.
2. While the strong force is the strongest natural force among the three fundamental forces, it has a short range many orders of magnitude smaller than electromagnetic force. As a result, the probability of neutrons interacting with a sample is very small, hence they are characterized by a deep penetration in the order of centimeters and they are less likely to damage a sample. In contrast, X-ray scattering is considerably more intense, but also has considerably less penetration, especially for metallic samples. The penetration is often between a few micrometers to a few hundred micrometers.
3. The neutron-nucleus interaction varies strongly with both the number of protons and the number of neutrons in a nucleus. Whereas X-ray scattering intensity is proportional to the number of electrons. One immediate consequence is the use of isotopic substitution technique available to neutron scattering. For the same chemical composition, isotopic substitution of an element has little to no effect on a range of physical properties investigated by scattering techniques, while providing a significantly different neutron scattering map that we can use to uniquely identify a particular atom or ion in a structure.
4. As a result of points 2 and 3 above, it is easier to study organic chemistry and biological materials with neutrons than with X-rays. Biological tissues can be very sensitive and easily damaged. These materials often contain low atomic number elements. This does not pose a challenge for neutron scattering, but it is challenge for X-ray scattering as the intensity is relatively speaking lower. Often a high-intensity X-ray source, such as a synchrotron X-ray source, is needed for a study. The use of high-intensity X-rays, however, may be too intense for higher atomic number constituents in the sample, and can damage the sample.
5. Since neutrons do not have an electric charge, but they still have a small magnetic moment, they are excellent for investigating the magnetic structure of materials. Any atomic or ionic magnetic moment would give rise to magnetic neutron scattering with the intensity of the magnetic scattering being proportional to the square of magnetic moments in the sample. In addition, using polarised neutron scattering, the directions of magnetic moments can be determined – a task difficult to achieve by conventional magnetometry techniques. The neutron magnetic moment is several orders of magnitude smaller than the atomic or ionic magnetic moments. The neutron magnetic scattering intensity is comparable to nuclear scattering intensity. This allows neutron

magnetic scattering to be a deep-penetrating, non-destructive technique.
In contrast, most X-ray magnetic scattering use resonance scattering technique that probes a specific magnetic moment. The complementarity of the two techniques is significant: neutron scattering can reveal all magnetic moments and the magnetic structure in a sample, while X-ray magnetic scattering is element specific. Often both techniques are employed to gain a better understanding of the magnetism in a material.

Owing to its ability to measure the chemical and magnetic structure and dynamics in the mesoscopic to nanoscopic length scales, and it being a non-destructive measurement tool, neutron scattering has found applications in virtually all aspects of material science research. For instance, in the study of biological phenomena, how a molecule of a medicine interacts with the cell membrane, the structure of the DNA, and the protein folding process, are some of the applications of neutron scattering. Neutron magnetic scattering has long been used to understand the physics of spintronics materials, and has directly contributed to developments such as high-density recording, and magnetic RAM. It has also contributed to the understanding of both low-Tc and high-Tc superconducting materials. Lately, research in batteries, solar cells and hydrogen fuel cells are some topics where neutron scattering has been employed. In several neutron scattering facilities, there are instruments dedicated for battery research or large-scale programmes for battery research, highlighting the significant contribution by neutron scattering to different types of studies.

One of the main challenges for neutron scattering compared to X-ray sources is that it is more difficult to provide a high intensity flux. A laboratory-based X-ray source typically delivers a flux of 10^7photons/(cm^{2}s) to a sample. This is comparable to the typical neutron flux of $10^6 - 10^9$neutrons/(cm^{2}s) at the sample position. Synchrotron X-ray sources typically deliver 10^{22}photons/(cm^{2}s). Increasing the neutron flux on sample has been one of the main reasons for building new neutron scattering facilities, upgrading existing neutron sources, and advancing neutron transport techniques such as neutron guides. The European Spallation Source, currently under construction, will be the latest and brightest neutron source in the world.

1.3 European Spallation Source (ESS)

The European Spallation Source (ESS) is being constructed in Lund, Sweden and planned to become a world leading research facility. The goal of ESS is to produce neutron beams with unprecedented intensity, with a pulse duration of the order of milliseconds and a frequency of 14 Hz. The purpose is to improve the availability of neutrons for scientific and technological studies. It is planned that the ESS facility will be operational in 2023 , as seen in Figure 1. The accelerator is planned to produce the highest intensity proton beam in the world, hitting a target to produce neutrons. The neutrons are then delivered to fifteen separate scientific instruments where they are used mostly for material analysis purposes. These instruments run simultaneously but each one of them focuses on particular types of research.

1.4 Neutron production

In the past, neutrons scattering research experiments were often performed at nuclear reactors. Nowadays there are also spallation sources which provide neutron beams with different characteristics. There are some essential differences between spallation sources and nuclear reactors.

Nuclear reactors produce neutrons as a result of nuclear fission where a nucleus is split into two fragments. About 2.5 neutrons are released per fission event and gamma radiation is produced as well. A significant amount of the energy in this process is dissipated, as kinetic energy of the fragments, into heat (~180 MeV per event). The neutrons are slowed down to an energy suitable for material science in moderators. Downstream at an instrument, neutrons with a certain wavelength are selected with the help of a monochromator, which works essentially in the same way as a diffraction grating, so that one can achieve a high intensity for a narrow wavelength range. The typical way to reduce the neutron flux, is by putting in control rods, which absorb the neutrons and stop the chain reaction.

Spallation sources produce neutrons with a reaction called spallation: the nucleus of a heavy element, such as Tungsten or Mercury, is hit by an incoming proton and becomes highly energetic. Subsequently the process leads to an intranuclear cascade, which essentially leads to a disintegration of the nucleus into smaller pieces. In this process, about 10-40 neutrons per incident proton are released and much less energy is dissipated into heat (~32 MeV) and gamma radiation. Similar to neutrons produced by a reactor source, moderators are used to lower the

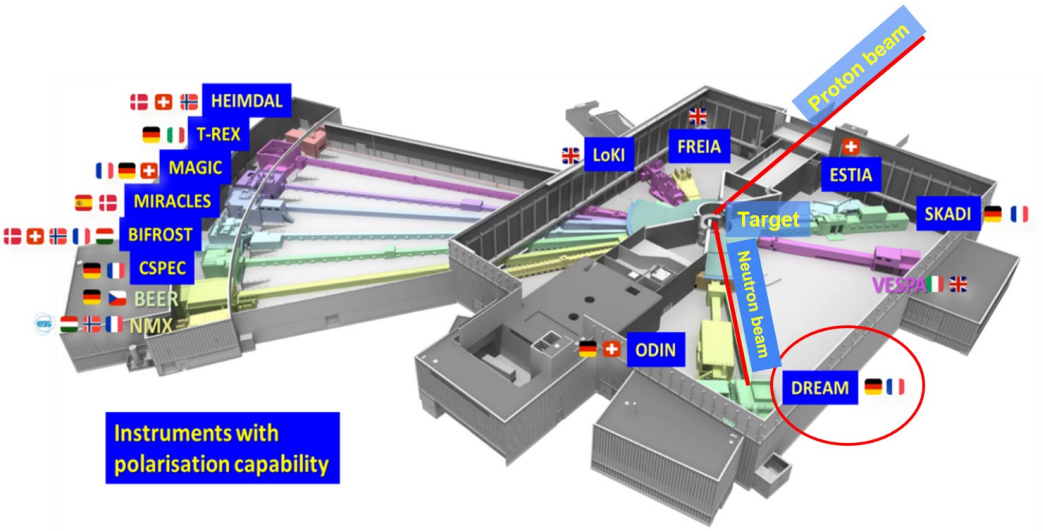

Figure 1: Schematics of ESS. In the center there is the Tungsten target which is bombarded by a pulsed proton beam and produces neutrons. These neutrons are delivered to the different instruments via neutron guides. On the bottom right one can see the DREAM instrument.

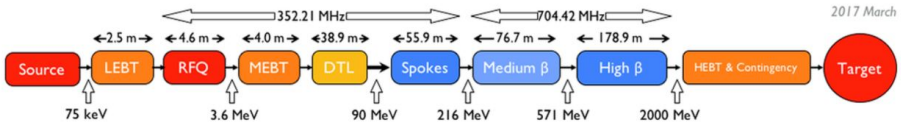

Figure 2: Schematic representation of proton accelerator at ESS. Reproduced from [3].

neutron energies to a range suitable for material science research [2].

The way neutrons are produced at ESS is indicated in Figure 2. Hydrogen gas is heated up by a electromagnetic field, so that the Hydrogen is ionized. The proton beam is then transported into the accelerator beam line through a Low Energy Beam Transport (LEBT) and reaches a linear accelerator (Linac). In the Linac electrodes are placed along the path of the accelerator, so that electrically charged particles are attracted or repelled. A Radio Frequency (RF) voltage is applied over a straight hollow pipe, and its polarity is changed when the ions cross the electrodes so that that the ions are always accelerated in the beam direction. The pipe is composed by a sequence of drift tubes made of electrodes which become progressively longer, in order to compensate for the fact that the particles acquire velocity [4].

The beam is focused and directed by means of magnets placed along the beamline (MEBT). In the last step of the accelerator superconducting cavities (Spokes) are used. The reason for using superconductors is that their very low electrical resistance minimizes electric losses enabling use of very high power. After further acceleration in the High Energy Beam Transport (HEBT) to 96% of the speed of light, the proton beam reaches the rotating target wheel, which is made of bricks of Tungsten and cooled with Helium.
In the target spallation reaction occurs and neutrons that travel at 10 % of the speed of light are released. These neutrons are then slowed down by a moderator so that they reach more or less the speed of sound, a speed which is suitable for material science studies. Afterwards, they are directed by supermirror guides and delivered to the various instruments.

1.5 DREAM diffractometer

The magnetic field setup to enable neutron polarisation analysis in the ESS instrument DREAM is the focus of this project. DREAM stands for Diffraction Resolved by Energy and Angle Measurements. DREAM is designed to ultilise the long-pulse characteristics of the ESS. Time-of-flight instruments at spallation neutron sources typically

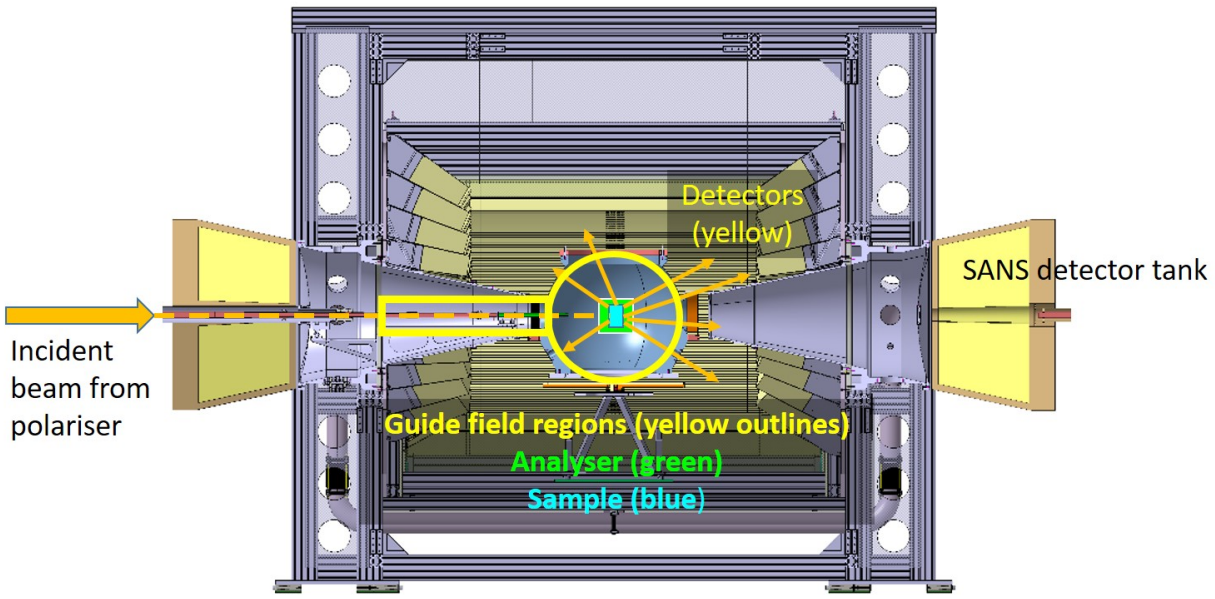

Figure 3: Schematic drawing of the DREAM sample and detector tank. The incident beam after the polariser (not shown) enters from the left and impinge upon the sample (blue). The scattered neutrons (orange arrows from the sample) are analysed by the polarisation analyser (green) and detected by the detectors. Guide field regions in the tank (yellow outsides) provide the spin-transport and the quantisation axis of neutron polarisation.

use the neutron flight time to achieve energy/wavelength resolution. Higher energy neutrons have a higher speed, and lower energy neutrons have a lower speed. As a result, a neutron pulse's longitudinal width increases as it travels along the flight path, with the leading edge containing the highest energy neutrons in the pulse and the trailing edge the lowest energy neutrons. Timing the arrival of the neutrons to the detector determines the neutron energy involved in the scattering process.

In a short-pulse neutron source, e.g., the Spallation Neutron Source (SNS) in the US, which has a pulse repetition rate of 60 Hz, two instruments are needed for diffraction studies. One located close to the source of the neutrons for high-intensity measurements that use all neutron pulses, and another one located further away for high-resolution studies. The reason for having two instruments is that the high-resolution instrument can only use every second neutron pulse to avoid "frame overlap" where the lower-energy neutrons in a pulse overlap with the higher-energy neutrons of the next pulse. At the ESS, which is a long-pulse neutron source with a repetition rate of 14 Hz, DREAM is designed to be located at a distance that can achieve both high-intensity and high-resolution in the same instrument (see Figure 3).

In a diffraction instrument, neutrons scatter from a sample into the full 4π solid angle. Within the engineering constraints, DREAM's sample-detector tank (see Figure 3), where scattering and detection occur, is covered by detectors in a cylindrical arrangement. In addition, a medium-range Small Angle Neutron Scattering (SANS) detector tank (only partly shown in Figure 3) downstream from the diffraction detector tank will be incorporated to reach the angular resolution needed by extending the range of the detectors.

To facilitate polarisation analysis for magnetic scattering studies, an additional setup is needed to condition the neutron beam and analyse the magnetic scattering. As we will discuss in more details in Section 2 below, the neutrons coming from the target need to be polarized first, since otherwise the scattering would not give the needed information. A polariser conditions the unpolarised beam to produce a polarised neutron beam that impinges on the sample. Upon scattering from a sample, the polarisation of the scattered neutrons are analysed by the polarisation analyser. The polarisation analyser converts the scattered neutrons' polarisation information into the corresponding intensities, which are then measured by the detectors. The polariser itself is provided by a different project. Here, we focus on the polarisation analyser.

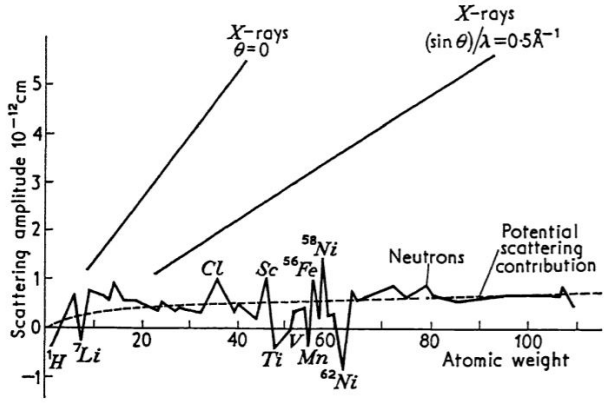

Figure 4: Scattering amplitude vs atomic weight for neutrons and X-rays for two different scattering angles. Note that this plot is simplified as X-ray scattering from ^{58}Ni and ^{62}Ni should have the same amplitude. Reproduced from [5].

2 Theoretical Background

2.1 Nuclear coherent scattering

Nuclear coherent scattering is the interaction between the neutron and the atomic nucleus due to the strong force. One can gain some understanding of this process by comparing with X-ray scattering. The probability amplitude of the scattering (scattering amplitude) is the outgoing wave divided by the incoming wave. X-ray scattering is described by an electromagnetic interaction between the photon and the electron. Its scattering amplitude is very sensitive to the scattering angle, as shown in Figure 4. The relation is described by the following expression that gives the scattering amplitude for a free electron in an electromagnetic field of amplitude H, at a distance r:

$$\text{Scattering amplitude} = H\frac{e^2 sin(\theta)}{m_e c^2 r} \tag{1}$$

where θ is the scattering angle, m_e the electron mass, e the electron charge, and c the speed of light. Maximum scattering is achieved for an angle of $\frac{\pi}{2}$. The X-ray scattering amplitude is also linearly proportional to the atomic number as shown in Figure 4 , since with higher atomic number there are more electrons that the X-ray can interact with.

Nuclear coherent scattering works differently. An incoming neutron beam travelling in the z direction, with wavelength λ, can be described by a plane wave:

$$\psi_i = e^{ikz} \tag{2}$$

where k= $\frac{2\pi}{\lambda}$ is the wave number. When the wave scatters on a single nucleus, which is a localized target when the neutron wavelength is larger than the size of the nucleus, the nucleus can be treated as an attractive or repulsive potential, depending on the case. The scattered wave has a spherical form:

$$\psi_r = -(\frac{b}{r})e^{ikr} \tag{3}$$

where b is the nuclear scattering length, and r the distance from the nucleus. Moreover, b > 0 means repulsive potential while b < 0 means an attractive potential. The scattered wave acquires a phase shift with respect to the incoming one. Negative scattering amplitude as in the case of Li in Figure 4 represents a phase difference of 180°.

One thing to be noted is that differently from X-ray scattering, nuclear coherent scattering from a nucleus is angle independent. We can thus define the cross section σ as the ratio between outgoing and the incoming currents:

$$\sigma = 4\pi r^2 v\frac{|(\frac{b}{r})e^{ikr}|^2}{v|e^{ikz}|^2} = 4\pi b^2 \tag{4}$$

where v is the neutron velocity. The cross section represents the likelihood of interaction.

In the case of multiple nuclei, constructive interference between the spherical waves is achieved when Bragg's law is fulfilled. Hence, this introduces the angular dependence of the scattering intensity. One often introduces two quantities: the structure factor $F(\boldsymbol{Q})$ and the differential cross section $\frac{d\sigma}{d\Omega}$. The structure factor tells if we achieve constructive interference. The differential cross section, which is defined as the modulus squared of the scattering amplitude, represents again the likelihood of interaction, but only for a fraction of the solid angle.
Following the derivation of general scattering theory [6], the differential cross section for neutron scattering for an incident neutron with wave vector, $\boldsymbol{k}_i$, to a scattered neutron with wave vector, $\boldsymbol{k}_f$, due to the interaction potential, V, is:

$$\frac{d\sigma}{d\Omega} = (\frac{m}{2\pi\hbar^2})^2 | < \boldsymbol{k}_f | V | \boldsymbol{k}_i > |^2 \tag{5}$$

and

$$< \boldsymbol{k}_f | V | \boldsymbol{k}_i > = \iint_V e^{i\boldsymbol{Q}\cdot\boldsymbol{r}} V(\boldsymbol{r} - \boldsymbol{R}) d\boldsymbol{r} d\boldsymbol{R} \tag{6}$$

with scattering vector, $\boldsymbol{Q}$= $\boldsymbol{k}_f - \boldsymbol{k}_i$, $\boldsymbol{r}$, is the position of the neutron, and $\boldsymbol{R}$ is the position of the nucleus or the magnetic moment. Equation 6 is the Fourier transform of the potential V. For a collection of nuclei at positions $\boldsymbol{R}_j$, with scattering length b, the potential, V, is known as the Fermi pseudopotential:

$$V(\boldsymbol{r}) = \frac{2\pi\hbar^2}{m} \sum_j b \cdot \delta(\boldsymbol{r} - \boldsymbol{R}_j) \tag{7}$$

with δ being the delta-function. Bragg's law comes from a regular placement of the nuclei on a lattice, the differential cross-section becomes:

$$|F(\boldsymbol{Q})|^2 = b^2 \sum_{\boldsymbol{G}} \delta(\boldsymbol{Q} - \boldsymbol{G}) \tag{8}$$

where $\boldsymbol{G}$ is the reciprocal lattice vector, and the delta function means that scattering only occurs when $\boldsymbol{Q}$ = $\boldsymbol{G}$. The magnitude of $\boldsymbol{G}$, $|\boldsymbol{G}|$=2π/d where d is the spacing between parallel planes formed by the nuclei in the lattice. With the scattering angle between $\boldsymbol{k}_f$ and $\boldsymbol{k}_i$ being ϕ, $|\boldsymbol{G}|$=$4\pi sin(\phi/2)\lambda$, where λ is the wavelength of the neutron. Bragg's Law λ=2d $sin(\phi/2)$ follows from $|\boldsymbol{Q}| = |\boldsymbol{G}|$.

Another expression for the cross-section can be given:

$$\sigma = 4\pi \left| \epsilon + \frac{constant}{(E - E_r) + \frac{i}{2}(\tau_n + \tau_a)} \right|^2 \tag{9}$$

here E is the neutron energy, and E_r the resonance energy determined by the details of the nuclear potential, which often can be approximated by a square well. τ_n and τ_a are the widths of the resonance for re-emission and absorption. One can see two terms in eq. (9), the potential scattering and the resonance terms. The potential term, ϵ, is proportional to the nuclear radius, R_n. This means that far from resonance (e.g., at low velocities) the cross section is purely given by $4\pi R_n^2$, which is reasonable as the larger the target is the higher the chance is to hit it. On the other hand, close to resonance the cross-section can increase significantly as can be seen in Figure 4. This occurs when quantum mechanics plays a role [5].

2.2 Magnetic scattering

The magnetic scattering arises from the interaction of the neutron magnetic moment and the magnetic field generated by the magnetic moment of atoms or ions. The interaction potential that gives rise to magnetic scattering is given by:

$$V_m = -\boldsymbol{\mu} \cdot \boldsymbol{B} \tag{10}$$

where $\boldsymbol{\mu}$ is the neutron magnetic moment and $\boldsymbol{B}$ is the magnetic field. Consider a single unpaired electron at position $\boldsymbol{R}$, and a neutron at position $\boldsymbol{r}$, with $\boldsymbol{u} = \boldsymbol{r} - \boldsymbol{R}$, the vector potential at the position of the neutron is:

$$\boldsymbol{A}(\boldsymbol{u}) = 4\pi\mu_0 \frac{\boldsymbol{\mu}_e \times \hat{\boldsymbol{u}}}{u^2} \tag{11}$$

where $\boldsymbol{\mu}_e$ is the magnetic moment of the electron. Introducing $\boldsymbol{B}$=$\nabla \times \boldsymbol{A}$ and the magnetic moment of the neutron into the interaction potential gives:

$$\frac{m}{2\pi\hbar^2} V_m = (\frac{\mu_0}{4\pi} \gamma \mu_N 2\mu_B \frac{m}{2\pi\hbar^2} 4\pi)\, \boldsymbol{s} \cdot \nabla \times \boldsymbol{M} \times \nabla \frac{1}{\boldsymbol{u}} = \gamma r_0 \boldsymbol{s} \cdot \nabla \times \boldsymbol{M} \times \nabla \frac{1}{\boldsymbol{u}} \tag{12}$$

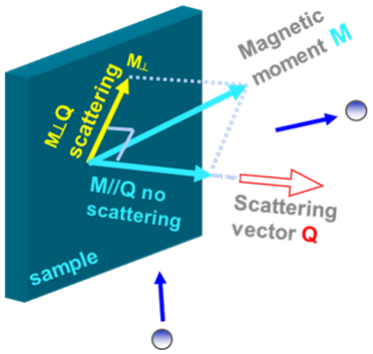

(a) First rule for magnetic scattering.

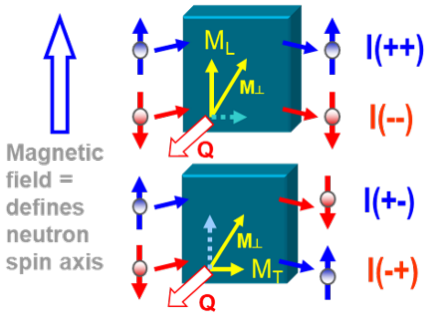

(b) Second rule for magnetic scattering.

Figure 5: Magnetic scattering rules: (a) only the magnetisation component perpendicular to the scattering vector contributes to magnetic scattering, (b) the magnetisation component parallel to the applied field contributes to non-spin-flip scattering, the magnetisation component perpendicular to the applied field contributes to spin-flip scattering.

where γ is the neutron gyromagnetic ratio, r_0 is the classical electron radius, $\boldsymbol{s}$ is the neutron spin, and $\boldsymbol{M}$ is the magnetisation. Considering the more general case of multiple magnetic moments, using the magnetic interaction potential in eq. (6) and taking into account the neutron spin, gives:

$$< \boldsymbol{k}_f, \boldsymbol{s}_f | V_m | \boldsymbol{k}_i, \boldsymbol{s}_i >= p f_M(Q) F_M(\boldsymbol{Q}) < \boldsymbol{s}_f | \boldsymbol{s} \cdot (\hat{\boldsymbol{Q}} \mathrm{x} \hat{\boldsymbol{M}} \mathrm{x} \hat{\boldsymbol{Q}}) | \boldsymbol{s}_i > \tag{13}$$

where p is the magnetic scattering length, f_M(Q) is known as the magnetic form factor, which is the Fourier transform of the electronic wavefunction, and $\hat{\boldsymbol{Q}}$ and $\hat{\boldsymbol{M}}$ are the unit vectors of $\boldsymbol{Q}$ and $\boldsymbol{M}$, respectively. $F_M(\boldsymbol{Q})$ is the structure factor that depends only on the locations of the magnetic moments. An immediate consequence of the factor $\hat{\boldsymbol{Q}}\mathrm{x}\hat{\boldsymbol{M}}\mathrm{x}\hat{\boldsymbol{Q}}$ is that the component of magnetisation $\boldsymbol{M}$ along the scattering vector $\boldsymbol{Q}$ is zero, and that only the component of the magnetisation that is perpendicular to the scattering vector contributes to magnetic scattering. This is our magnetic scattering rule 1 (see Figure 5). Let $\boldsymbol{m}\perp = \hat{\boldsymbol{Q}}\mathrm{x}\hat{\boldsymbol{M}}\mathrm{x}\hat{\boldsymbol{Q}}$, we now consider the effect of the direction of neutron spins. Neutrons are spin 1/2 particles with two possible spin states: +, with the spin parallel to the magnetic field direction and - with the spin anti-parallel to the field (using the magnetic field as quantization axis). If we choose the coordinates such that the applied field is along the +z direction, then there are four possible spin state transitions that the scattering can lead to:

$$< + | \boldsymbol{s} \cdot \boldsymbol{m}\perp | + >= m\perp_z \tag{14}$$

$$< - | \boldsymbol{s} \cdot \boldsymbol{m}\perp | - >= -m\perp_z \tag{15}$$

$$< + | \boldsymbol{s} \cdot \boldsymbol{m}\perp | - >= m\perp_x + i m\perp_y \tag{16}$$

$$< - | \boldsymbol{s} \cdot \boldsymbol{m}\perp | + >= m\perp_x - i m\perp_y \tag{17}$$

which means that magnetic scattering can either be spin-flipping (SF) or non-spin-flipping (NSF). This gives magnetic scattering rule 2 (see Figure 5 (b)): The component of $\boldsymbol{m}\perp$ that is collinear with the applied magnetic field gives rise to non-spin-flip scattering, and the component of $\boldsymbol{m}\perp$ that is perpendicular to the applied field gives rise to spin-flip scattering.
Since there are two possible types of scattering (nuclear and magnetic), the interaction potential is the sum of the two:

$$V = V_N + V_m. \tag{18}$$

One can get a further understanding by looking at basic examples of magnetic scattering in a ferromagnetic material.
Case 1: The ferromagnetic moment, $\boldsymbol{M}$, is perpendicular to the scattering vector, $\boldsymbol{Q}$. The applied field is along the ferromagnetic moment, i.e. $m\perp_z = 1$, $m\perp_x = m\perp_y = 0$. For ferromagnets, the structure factor for the atomic nuclei and the magnetic moments are the same, giving

$$< + | V_N + V_m | + >= (b + p f_M(Q)) F(\boldsymbol{Q}) \tag{19}$$

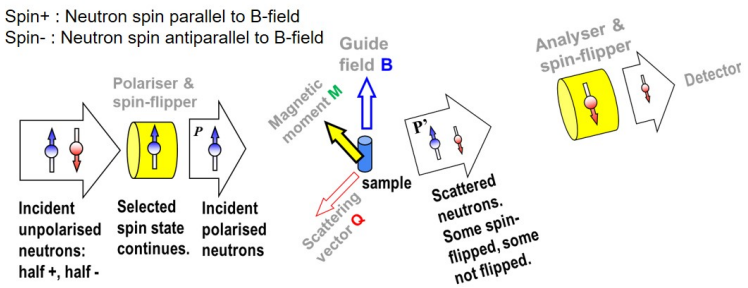

Figure 6: Schematic representation of magnetic scattering.

$$< -|V_N + V_m| - >= (b - pf_M(Q))F(\boldsymbol{Q}) \tag{20}$$

$$< +|V_N + V_m| - >= 0 \tag{21}$$

$$< -|V_N + V_m| + >= 0. \tag{22}$$

This tells us that the scattering in this arrangement is entirely non-spin flip. Moreover, depending on the polarisation of the incident neutron, the scattering peak intensity either increases or decreases. In fact, one can arrange to make a material so that the averaged scattering lengths satisfy $b = pf_M(Q)$, so that the neutrons in one spin state will be scattered while those in the other spin state will go through without interaction. This is the basis of crystalline based neutron polariser. The same principle applies to polarising supermirrors.
Case 2: The ferromagnetic moment, $\boldsymbol{M}$, is perpendicular to the scattering vector, $\boldsymbol{Q}$. The applied field is along $\boldsymbol{Q}$, i.e., perpendicular to the ferromagnetic moment, i.e., $m\perp_z = 0$, $m\perp_x^2 + m\perp_y^2 = 1$

$$< +|V_N + V_m| + >= bF(\boldsymbol{Q}) \tag{23}$$

$$< -|V_N + V_m| - >= bF(\boldsymbol{Q}) \tag{24}$$

$$< +|V_N + V_m| - >= pf_M(Q)(m\perp_x + im\perp_y) \tag{25}$$

$$< -|V_N + V_m| + >= pf_M(Q)(m\perp_x + im\perp_y) \tag{26}$$

For collinear magnetic moments, $< +|V_N + V_m| - > = < -|V_N + V_m| + > = p^2 f_M^2(Q)$. All NSF scattering are nuclear scattering and all SF scattering are magnetic scattering.

2.3 Magnetic scattering in DREAM

In a typical magnetic scattering experiment, as shown in Figure 6, unpolarised neutrons are first filtered according to their spin in the polariser. After they scatter against the sample, they reach the polarisation analyser. As discussed in section 2.2, this scattering can be either SF or NSF, depending on the sample structure and on the angle of incidence of the neutrons with the respect to the magnetization of the sample. The scattered neutrons are then filtered again according to their spin by the polarisation analyser and measured by a detector.

In the instrument DREAM, a magnetic field provides the spin-transport of the neutrons to the sample and the analyser, which is composed by a tetracoil that contains a ^{3}He cell with polarized ^{3}He gas, and is surrounded by neutron detectors. Some neutrons will not scatter and they will continue moving to the right in Figure 6. Some will scatter and might then hit the ^{3}He cell which covers a portion of the solid angle. Then the neutrons with spin antiparallel to the ^{3}He nuclear spin will bond and be absorbed, while the ones with parallel spin will reach the detector. One can understand the reason why it is necessary to have an analyser. The detector is based on unpolarized ^{3}He and cannot tell the difference between a neutron with spin up or down. Hence without an analyser the counts in the detector do not provide us with any useful information related to the structure of the sample.

The reason why the ^{3}He cell does not cover the full solid angle is that the ^{3}He gas has to be polarized before being injected into the cell. It takes approximately one hour for the filling of a 1 l ^{3}He cell and in this time the ^{3}He gas continues to lose its polarization. Hence too large a coverage of the solid angle only leads to a large loss of polarization.

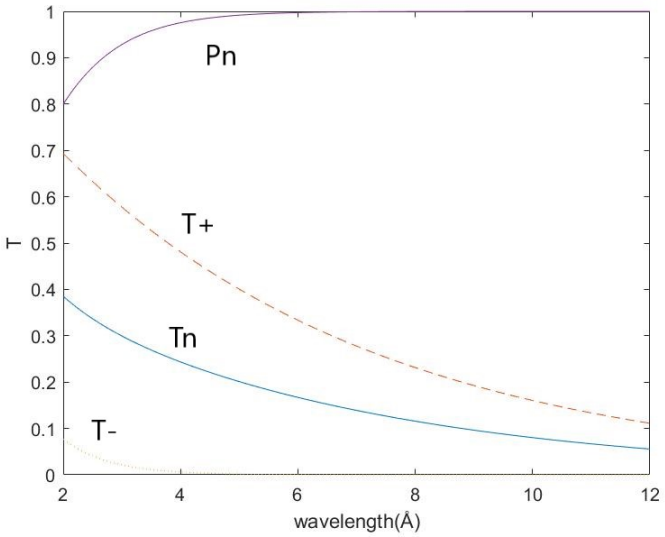

Figure 7: Neutron transmission probabilities and polarization vs wavelength for a ^{3}He polarization of 80% and the length of the cell 10 cm.

The magnetic field design was made in order to mainly fulfill two purposes. First, the field has to be uniform enough such that the neutron spin-transport is adiabatic, i.e., to ensure the neutron beam does not lose its polarization. Secondly, the field gradient has to be very small in the ^{3}He cell, in order to avoid that the ^{3}He immediately loses its polarization, which would destroy the neutron spin-filtering.

2.4 Neutron spin filtering with polarized ^{3}He

Different techniques can be used to spin-filter neutrons, e.g., supermirrors as mentioned in section 2.2, or a magnetic field gradient as in the Stern–Gerlach experiment. The method used in this project is based on polarized ^{3}He due to its strong spin dependent neutron absorption cross-section [7].

The neutron capture on ^{3}He results in a broad (Γ = 270 keV) intermediate unbound resonance state ($J^\pi = 0^+$) in ^{4}He (^{3}He + n $\rightarrow$ ^{4}He*), which decays to a tritium nucleus and a proton with an energy release of 740 keV. The ^{3}He nucleus consists of two protons and one neutron, where in a single particle picture the spin of the nucleus comes from the unpaired neutron. In the absorption process, a neutron with the spin component antiparallel to the ^{3}He nuclear spin has very large capture cross section ($\sigma \uparrow\downarrow$ [barn] $\approx 6000 \cdot \lambda$ [Å]) and is absorbed in the reaction, neglecting the small potential absorption of the neutrons with the spin component parallel to the ^{3}He nuclear spin ($\sigma \uparrow\uparrow \approx 5$ barn). In the end state the two neutrons have antiparallel spin due to the Pauli exclusion principle. It can be interesting to know that the tritium nucleus finally decays back to ^{3}He with a half life of $\approx$ 12 years. The transmission probabilities and the neutron polarization can be described by the following empirical relations:

$$T\pm = e^{-(1\mp P_{He})n_{He}\cdot\sigma(\lambda)\cdot l} \tag{27}$$

$$T_n = \frac{T_+ + T_-}{2} = e^{(-O)}\cosh(O\cdot P_{He}) \tag{28}$$

$$P_n = \frac{T_+ - T_-}{T_+ + T_-} = tanh(O\cdot P_{He}) \tag{29}$$

T$\pm$ is the transmission probability for neutrons with spin parallel and anti-parallel respectively, T_n is the transmission for unpolarized neutrons, P_{He} the Helium polarization, and O the opacity. Moreover, the opacity is defined as $n_{He}\cdot\sigma(\lambda)\cdot l$, where n_{He} is the density of Helium atoms, $\sigma(\lambda)$ the absorption cross section, which is proportional to the neutron wavelength, and l the length of the cell. Note that in practice $T+ \neq 1$ due to the finite polarization of ^{3}He [8].

As shown in Figure 7, the transmission for an anti-parallel spin is significantly smaller than that for parallel

spin. Moreover, they both decrease for increasing wavelength, as with lower neutron kinetic energy, the interaction time between the neutron and the Helium nucleus will be longer. One consequence of this is the fact that the polarization efficiency increases for increasing wavelength.

The advantage of using polarized ^{3}He for neutron spin-filtering is that it is flexible, and independent on whether the neutrons are cold or hot one can get an optimal transmission by tuning the pressure of the Helium. Other methods, e.g., supermirrors can be excellent for cold neutrons [7].

2.5 Neutron spin-transport in magnetic fields

If one considers a free neutron in a constant and uniform magnetic field pointing in the z direction, the neutron possesses a magnetic moment due to its spin, and hence the field will exert a torque on this magnetic moment.
By solving the time-dependent Schrödinger equation, it can be shown that the expectation value of the spin in the z direction $<\psi|s_z|\psi>$ is constant, while for the x and y directions we get:

$$<\psi|s_x|\psi> \propto cos(\omega_L t + \alpha) \tag{30}$$

$$<\psi|s_y|\psi> \propto sin(\omega_L t + \alpha) \tag{31}$$

These equations show that the neutron magnetic moment is precessing around the z axis. ω_L is called the Larmor frequency and describes the angular frequency of the precession while α is a phase constant [9] .
Moreover we can define the neutron beam polarization, $\boldsymbol{P}$, for a number, N, of neutrons as follows:

$$\boldsymbol{P} = \frac{1}{N}\sum_{i}^{N}\langle \boldsymbol{s} \rangle_i \tag{32}$$

This means that $|\boldsymbol{P}|$ will always have a value between 0 and 1. In particular, $|\boldsymbol{P}| = 1$ would mean that the neutron beam is 100% polarized.
In the case where the magnetic field is non uniform one talks about neutron adiabaticity. If the direction of the field changes too fast with respect to the Larmor precession, the neutron beam loses its polarization, and otherwise it maintains its direction of precession with respect to the field. The adiabaticity, A, tells in which of these two cases we are. For a neutron beam moving along the x direction it is defined as:

$$A = \frac{\omega_L}{\omega_B} = \frac{|\gamma||\boldsymbol{B}|}{v_n(d\theta_B/dx)} \tag{33}$$

where ω_B is the change of the field in the frame of reference of the neutron, $d\theta_B/dx$ the gradient of the field direction, γ the neutron gyromagnetic ratio, and v_n the neutron velocity [10]. A>10 is the condition for good spin transport. Moreover one can see that for a cold neutron, i.e., at low kinetic energy, it is easier to meet this condition than for a hot neutron.

2.6 Uniform magnetic fields with coils

As mentioned in section 2.4, for the purpose of this project it is essential for the ^{3}He to stay polarized. The problem is that the ^{3}He tends to lose its polarization over time according to the following equation:

$$P_{He}(t) = P_{He}(0)e^{-\frac{t}{T_1}} \tag{34}$$

where $P_{He}(0)$ is the initial ^{3}He polarization and T_1 the longitudinal spin relaxion time constant, which is typically about 100 - 300 hours.

In a magnetic field, $\boldsymbol{B} = B\hat{\boldsymbol{h}}$, where B is the field amplitude and $\hat{\boldsymbol{h}}$ the unit vector of field direction. With $\hat{\boldsymbol{h}}$ along the z direction, the longitudinal spin relaxion time constant is defined as:

$$\frac{1}{T_1} = D\frac{|\nabla h_x|^2 + |\nabla h_y|^2}{B^2} \tag{35}$$

where ∇h_x and ∇h_y are the field gradients, and D is the diffusion constant, which is inversely proportional to the ^{3}He pressure [11].

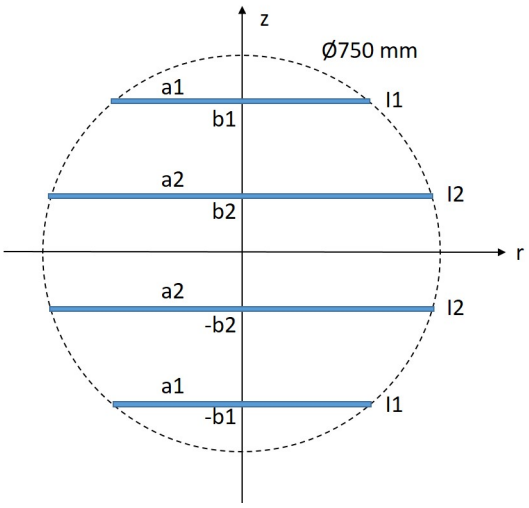

Figure 8: Schematics of a tetracoil. The double lines represent the position of the coils.

This implies that one way to slow down this process is to place the ^{3}He cell in a magnetic field that is as uniform as possible. The field uniformity u is defined by:

$$u = \max(J(\hat{\boldsymbol{h}}) \cdot \hat{\boldsymbol{v}}) \tag{36}$$

where $J(\hat{\boldsymbol{h}})$ is the Jacobian of magnetic field direction $\hat{\boldsymbol{h}}$, and $\hat{\boldsymbol{v}}$ is a unit vector of an arbitrary direction. The smaller u is, the more uniform the field is. In particular, u = 0 would mean an ideal field that is perfectly uniform [12].

One could think of a solenoid as the simplest solution to achieve a highly uniform magnetic field. However, since it is not practical to introduce a sample inside of a solenoid, coils appear to be the best solution. One could guess that a Helmoltz coil would be a good solution, as it can provide a wide region of field uniformity. However, the tolerance is ~ to 10 %, which is not too large for the purpose of this project. It is shown in the literature [13] that in order to achieve a region of uniformity, with a tolerance of ~0.1 %, there are two possible coil combinations. One is a tetracoil. Such a system is composed of four circular coils inscribed in a sphere, with two couples of coils of different widths, which are symmetrical with respect to the center of the sphere [13]. The other one is a system of four equally spaced square coils inscribed in a cube [14].

In this project a tetracoil is used. It is necessary to introduce a few parameters in order to describe such a structure (see Figure 8). In the following, i = I_1/I_2 where I_1 and I_2 are the number of turns for each couple of coils; $q = a_1/a_2$ where a_1 and a_2 are the radii of the external and of the internal coils, respectively. $\beta_1 = b_1/a_1$ where b_1 is the distance from the center of the external coils and a_1 its radius; $\beta_2 = b_2/a_2$ where b_2 is the distance from the center of the internal coils and a_2 its radius [13]. It can be shown that in order for a tetracoil to work in an optimal regime the parameters have to be set in the following way: $i = 0.6822$, $q = 0.6718$, $\beta_1 = 1.1880$, $\beta_2 = 0.2975$. A derivation of this result can be found in [13].

Another structure that has been essential for the purpose of this project is the Halbach four-coil [15]. This assembly consists of four rectangular coils located in the vertices of a square as shown in Figure 9. In a Halbach coil arrangement, if the angle between the central field axis and the line connecting the origin and the centre of a coil is χ, the angle between the central field and the field of that coil is 2χ. In the arrangemnt in Figure 9, starting from the central field axis, the coils are located at χ=45°, 135°, 225°, and 315°, respecively, and the coil field axis are at 90°, 270°, 450°(i.e., 90°), and 630°(i.e., 270°) from the central field axis. All coils have the same field amplitude. The Halbach 4-coil has the characteristics of having a large uniform field region at the centre and a rapidly decreasing field away from the coil assembly. The latter is due to the fact that the fields produced by the four coils cancel out as the distance from the coils increases. One could increase the number of coils and have an eight-coil system. In such system, the field would rotate 90° between neighbouring coils, and would further cancel out with a more rapid decrease in field strength outside the coil assembly. Extrapolating to an infinite number of coil elements, the field

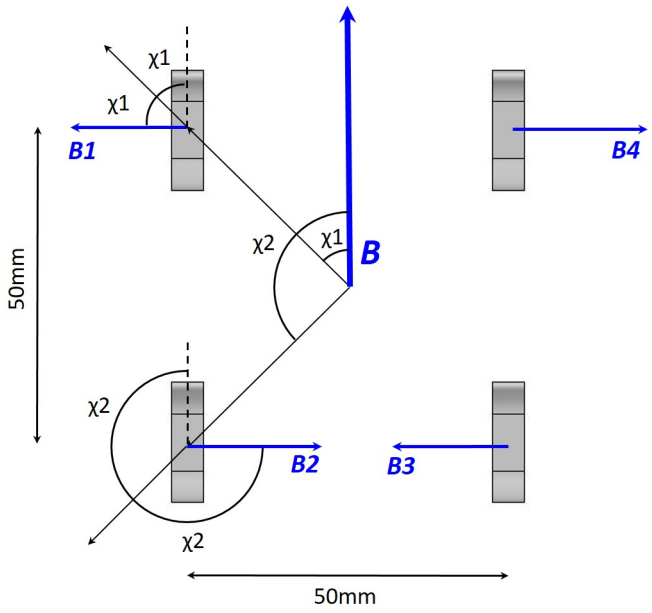

Figure 9: Schematic drawing of Halbach four-coil (grey) viewed from the front. In our model, the coil centers are located on a square of 50 mm x 50 mm. Shown in the figures are the central field $\boldsymbol{B}$, coil fields $\boldsymbol{B1} - \boldsymbol{B4}$, the angle from the axis of the central field to the line connecting the original and the centre of coil 1 is χ_1, and to the line connecting the original and the centre of coil 2 is χ_2. Also shown are the angle between $\boldsymbol{B}$ and $\boldsymbol{B1}$ which is $2\chi_1$ and between $\boldsymbol{B}$ and $\boldsymbol{B2}$ which is $2\chi_2$, respectively. The four coils have the same field strength.

would be perfectly uniform inside and exactly zero outside.

In order to study the uniformity of a magnetic field, the following concepts need to be introduced. One defines $\hat{\boldsymbol{v}}$ to be the unit vector related to a space displacement, and u to be the corresponding change of the directional vector of the magnetic field. The direction of the magnetic field is described by a vector field and its Jacobian is:

$$J = \begin{pmatrix} \nabla h_x \\ \nabla h_y \\ \nabla h_z \end{pmatrix}.$$

In order to estimate how much the field varies, the task is to find $\hat{\boldsymbol{v}}$ such that u^2 is maximized:

$$u^2 = (\nabla h_x \cdot \hat{\boldsymbol{v}})^2 + (\nabla h_y \cdot \hat{\boldsymbol{v}})^2 + (\nabla h_z \cdot \hat{\boldsymbol{v}})^2 \tag{37}$$

In the 1-D case it is trivial to solve the problem:

$$\hat{\boldsymbol{v}} = \frac{\nabla h}{|\nabla h|} \tag{38}$$

In the 3-D case on the other hand, it is impossible to analytically find a solution. Hence, the simplest approach is to find an overestimation of the change of the field by considering separately the components in the different directions:

$$u^2 = |\nabla h_x|^2 + |\nabla h_y|^2 + |\nabla h_z|^2 \tag{39}$$

We will refer to this expression as the magnetic field direction angular gradient. Following the convention in literature, it is given in the unit of rad/m.

3 Method

3.1 Finite Element Method

The Finite Element Method (FEM) is a numerical method used to approximate differential equations (often partial differential equations) that cannot be solved analytically. One way to do this is to use the Galerkin method, which

comprises various steps. The first one is the discretization of the domain, which means that the domain of the original equation gets split into different local domains. The next step is to approximate the solution by rewriting it as a linear combination of a mesh. One can consider the differential equation:

$$L(f(x)) = g(x) \tag{40}$$

where L is the differential operator, and f(x) the exact solution. One can then find an approximate solution F(x):

$$F(x) = \sum_{i}^{N} a_i \psi_i(x) \tag{41}$$

where $\psi_i(x)$ is the weight function or the mesh and a_i the coefficients to be determined. By inserting the approximate solution into the original differential equation, one gets the residual, R(x):

$$R(x) = L(F(x)) - g(x) \tag{42}$$

The residual represents the deviation between the approximate solution and the actual one. Hence, the task is to find the coefficients, a_i, such that the residual is minimized. The way to approach this is analogous to the least square method.
If one has a set of datapoints and wants to fit them to a linear relationship, the idea is to choose the line such that the sum of the distances squared between the model and the datapoints is minimized. That requires for the derivative of the summation to be 0. The Galerkin method is conceptually the same, it consists of taking the inner product of the residual and the weight functions and set it to 0:

$$\int_{x_1}^{x_2} R(x)\psi_j(x) = 0 \tag{43}$$

where x_1 and x_2 are the boundaries of the local domain. The same is done for all the local domains, and one can derive the stiffness matrix:

$$\underbrace{\begin{pmatrix} m11 & m12 & & & & \\ m21 & m22 & m23 & & & \\ & m31 & m32 & m33 & & \\ & & & \ddots & & \\ & & & & m_{n,n-1} & m_{n,n} \end{pmatrix}}_{\text{Stiffness matrix}} \begin{pmatrix} a_1 \\ a_2 \\ a_3 \\ \vdots \\ a_n \end{pmatrix} = \underbrace{\begin{pmatrix} b_1 \\ b_2 \\ b_3 \\ \vdots \\ b_n \end{pmatrix}}_{\text{Load vector}}$$

which contains the numerical solution to the problem. The reason why it is called the stiffness matrix is that this method was first used for structural mechanics purposes.

3.2 Evolution of magnetic field uniformity

COMSOL Multiphysics is a FEM based simulation software. It can be used to simulate different types of physics, e.g. acoustics or heat flow. In this project it has been used for the design of magnetic fields.
Every simulation in Comsol can be divided into the following steps. First the model environment is set up, which means to choose the spatial dimensions, the physics that will be investigated, and the type of study to be carried out. In this project a stationary study of magnetic fields was performed.
The next step is to build the starting geometry, which in this case it consists of the tetracoil, the guide field and the He cell. The tetracoil was designed according to the parameters given in section 2.6. The detector had been previously designed in a Computer-Aided Design (CAD) software called SolidWorks [16]. Consequently it was necessary to take some measurements and ensure that the new geometry would fit with the pre-existing one. The tetracoil was built with a diameter of 750 mm, while the guide field coils with a length of 550 mm. Three different setups were investigated and compared. The initial one, shown in Figure 10 (a) and (b), consists of the tetracoil and four rectangular square coils. The second one, in Figure 10 (c) and (d), has four extra nested rectangular coils. The last one, in Figure 10 (e) and (f), replaces the rectangular coils with a Halbach four-coil. For all the setups it was necessary to find optimal values for the current and size of the coils, as well as for the distance between the tetracoil and the guide field coils.
The material properties are also specified. The tetracoil and guide field coils were specified as made of copper, while the rest of the setup was set to air.

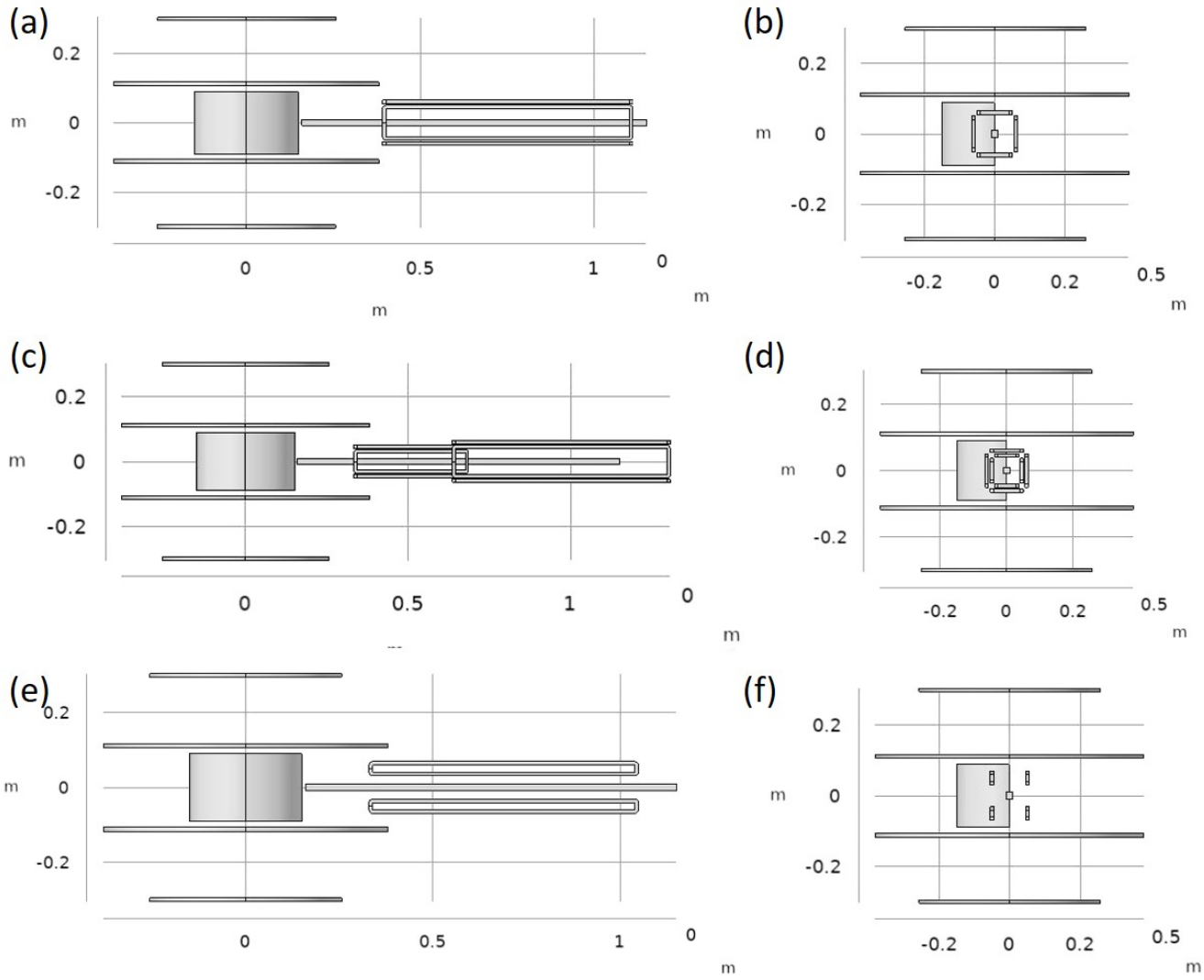

Figure 10: Representation of the initial setup, including tetracoil and four rectangular coils in (a) and (b). Representation of the nested setup, including tetracoil and eight nested rectangular coils in (c) and (d). Representation of the Halbach setup, including tetracoil and Halbach four-coil in (e) and (f). (a), (c), and (e) correspond to the XZ views of the mentioned setups, while (b), (d), and (f) correspond to the YZ views.

One also defines the physics boundary conditions, including defining the coils, the currents, and the number of turns. The tetracoil was set to a current of 5 A over all the coils, while the number of turns was set to 73 in the outermost coils and 73/0.688 = 107 in the innermost ones. The parameters of the tetracoil were kept the same through all the simulations. A very important step is to build the mesh, which in 3D typically is defined by tetrahedrals. The finer the mesh is the more accurate the solutions are. However, a finer mesh requires longer computation time. In general the size of the mesh should be smaller than the size of the objects in the simulation. Six different meshes were built:

	neutron tube	^{3}He cell	cell envelope	coils	coil space	remaining
mesh type	extremely fine	extremely fine	extremely fine	extremely fine	extra fine	normal
maximum size (m)	0.01	0.005	0.01	0.05	0.164	0.469

In this case two different studies were done. The first one simulated the magnetic field, the second one was performed in order to calculate the angular gradient of the magnetic field direction. It is necessary to post-process the results [17]. This was done by plotting the magnetic field, the magnetic field direction angular gradient, given by eq. (39), and the neutron adiabaticity, given by eq. (33), for a neutron wavelength of 1.5 Å.

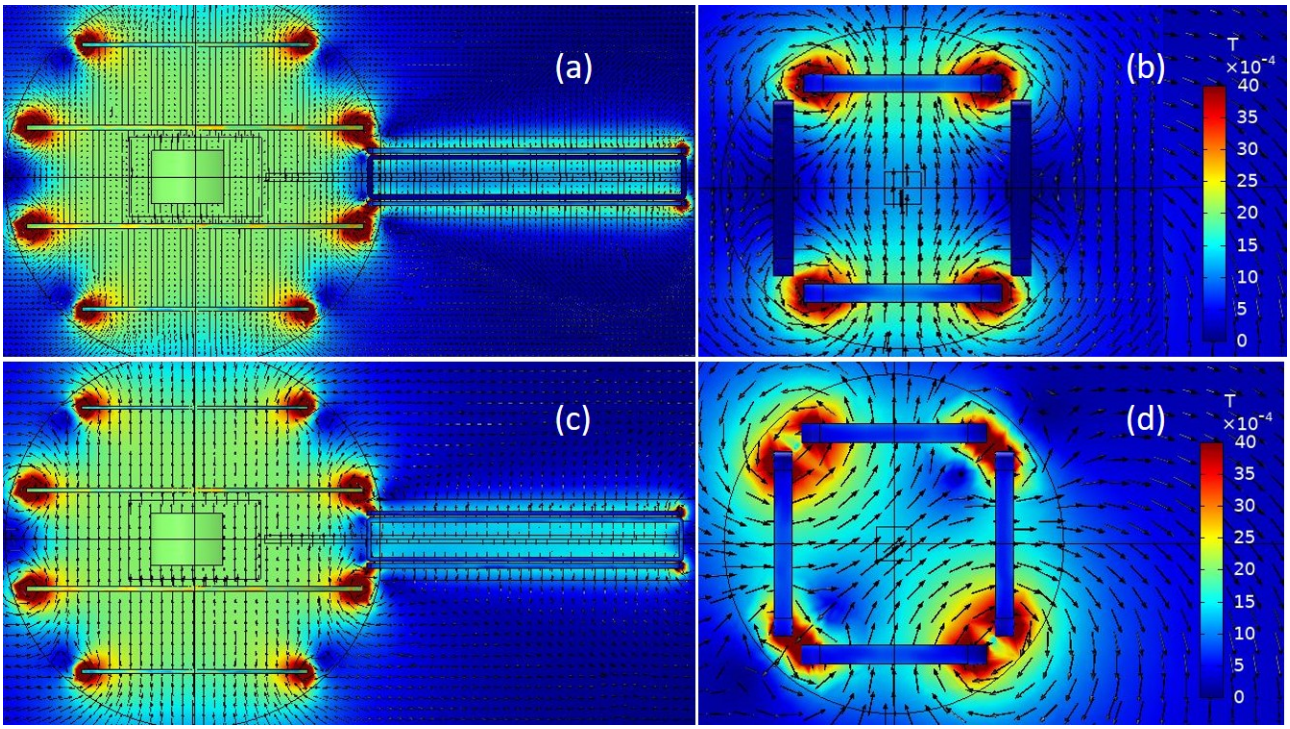

Figure 11: Magnetic field in a section of the tetracoil and of the guide field coils on the left, and in a section of the guide field coils on the right. The color represents the intensity of the field, the arrows the direction. The rectangular coils were set with a size of 80 mm and a current of 2 A. The distance between the He cell and the guide field coils was set to 40 cm. In (a) and (b) for current only in the vertical guide field coils, while in (c) and (d) for current in all the guide field coils.

The following specifications needed to be fulfilled. Firstly, it was necessary for the neutron adiabaticity A (eq. 33) to be above 10 over the full neutron flight path. Secondly, it was required for the magnetic field direction angular gradient to be below $5 \cdot 10^{-4}$rad/cm over the whole volume of the ^{3}He cell. The reason for choosing a wavelength of 1.5 Å is that the neutrons used at DREAM have wavelengths that range from 1.5 Å - 20 Å. As mentioned in section 2.5, if neutrons with the lowest possible wavelength fall into the adiabatic approximation, then all the others will as well.

4 Results and Analysis

4.1 First-cut design of magnetic field

In order to preliminary check if the structure was correctly designed, simulations of the magnetic field with the original setup were performed without any further calculation. The results shown in Figure 11 were obtained. As can be seen from the alignment of the field lines, and from the field map (apart from the outermost part), the field appears to be uniform and the geometry correctly built. The tetracoil is very sensitive to variations in its structure. If there were mistakes in its design, the field would not be uniform. The uniformity of the magnetic field was estimated to be about ~0.1 %, which, as mentioned in section 2.6, is in agreement with previous literature concerning tetracoils. The uniformity of the field at the ^{3}He cell can be seen in Figure 12. The magnetic field direction angular gradient is less than $5 \cdot 10^{-4}$rad/cm at the cell. However, there is little margin left.

The currents in the coils were chosen such that the magnetic fields in the tetracoils and in the guide field coils would have comparable magnitude. However, one can observe that the field is not uniform in the interface between the tetracoil and the guide field. This problem will be addressed below in the refinement of the model. This is also

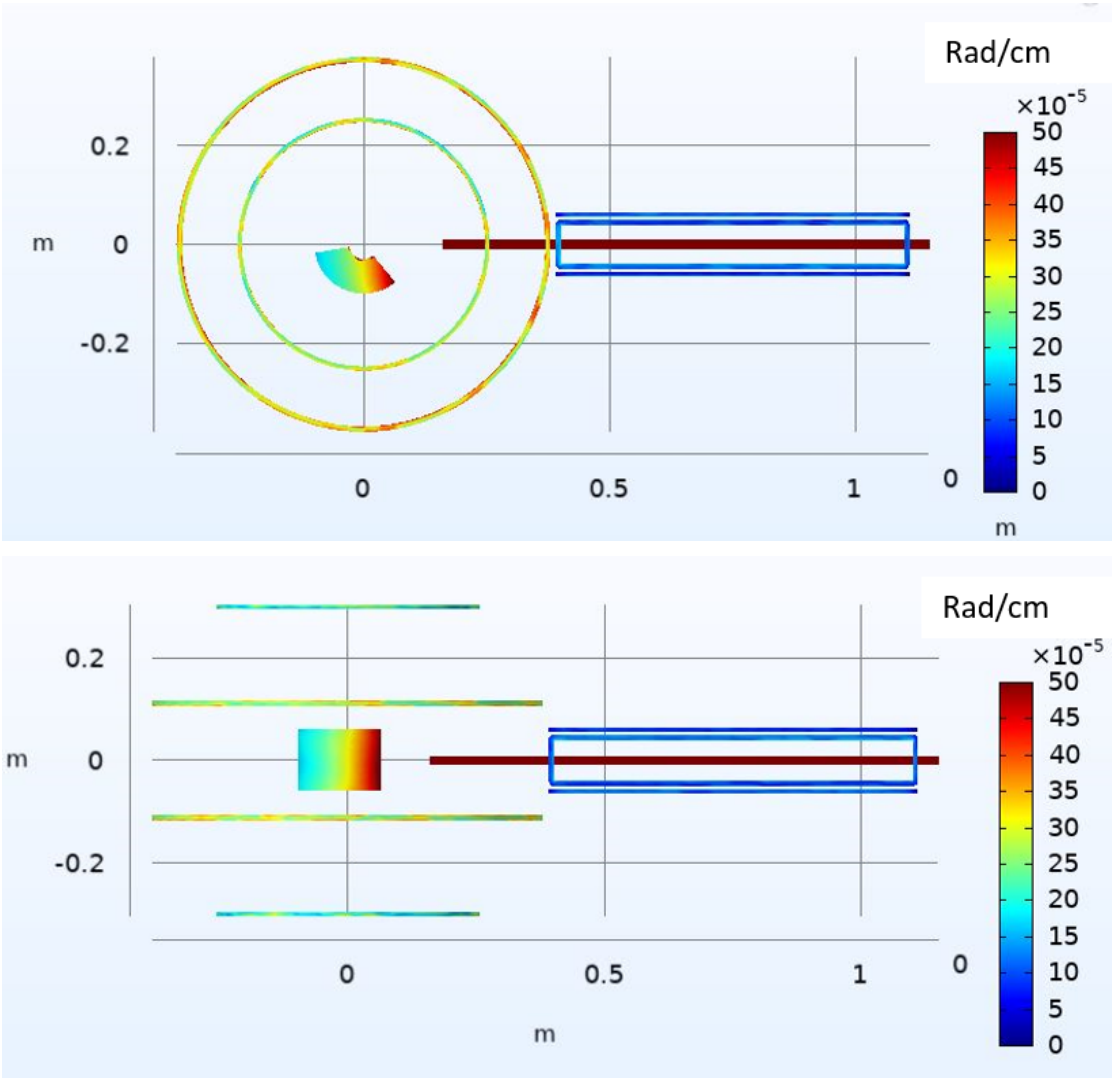

Figure 12: Magnetic field direction angular gradient in the ^{3}He cell for the initial setup. XY view on top and XZ view on the bottom

the reason why it was necessary to investigate different setups.

4.2 Refinement of the model

4.2.1 Initial setup

As can be observed in Figure 13, the initial setup, see Figure 10 (a) and (b), has a significant limitation. The transport is excellent in the tetracoil region, and in the guide field, but non-adiabatic in the interface between the two. This means that a neutron beam would lose its polarization when passing through that region. One could think as a solution to move the guide field coils inside the tetracoil, but unfortunately that cannot be done. As shown in Figure. 14 on top, the angular gradient of the magnetic field direction in the ^{3}He cell is higher the closer it gets to the guide field coils. This means that the magnetic field in the tetracoil is strongly disturbed by the magnetic field generated by the rectangular coils. Given this, to move the guide coils even closer to the ^{3}He cell, would influence the ^{3}He polarization even more, i.e., the gradient in the He cell would increase as shown in Figure 14 on top.

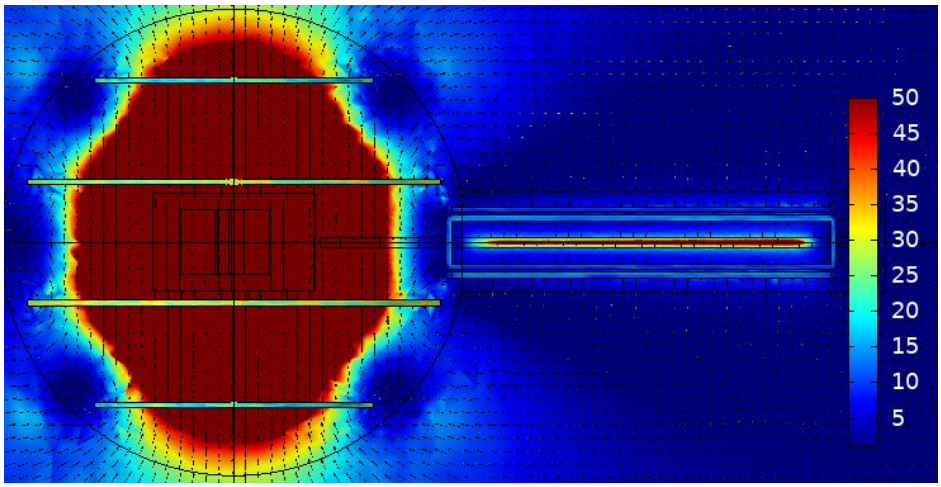

Figure 13: Neutron adiabaticity for the initial setup. The guide field coils were set to a size of 80 mm and a current of 2 A. The distance between the He cell and the guide field coils was set to 40 cm.

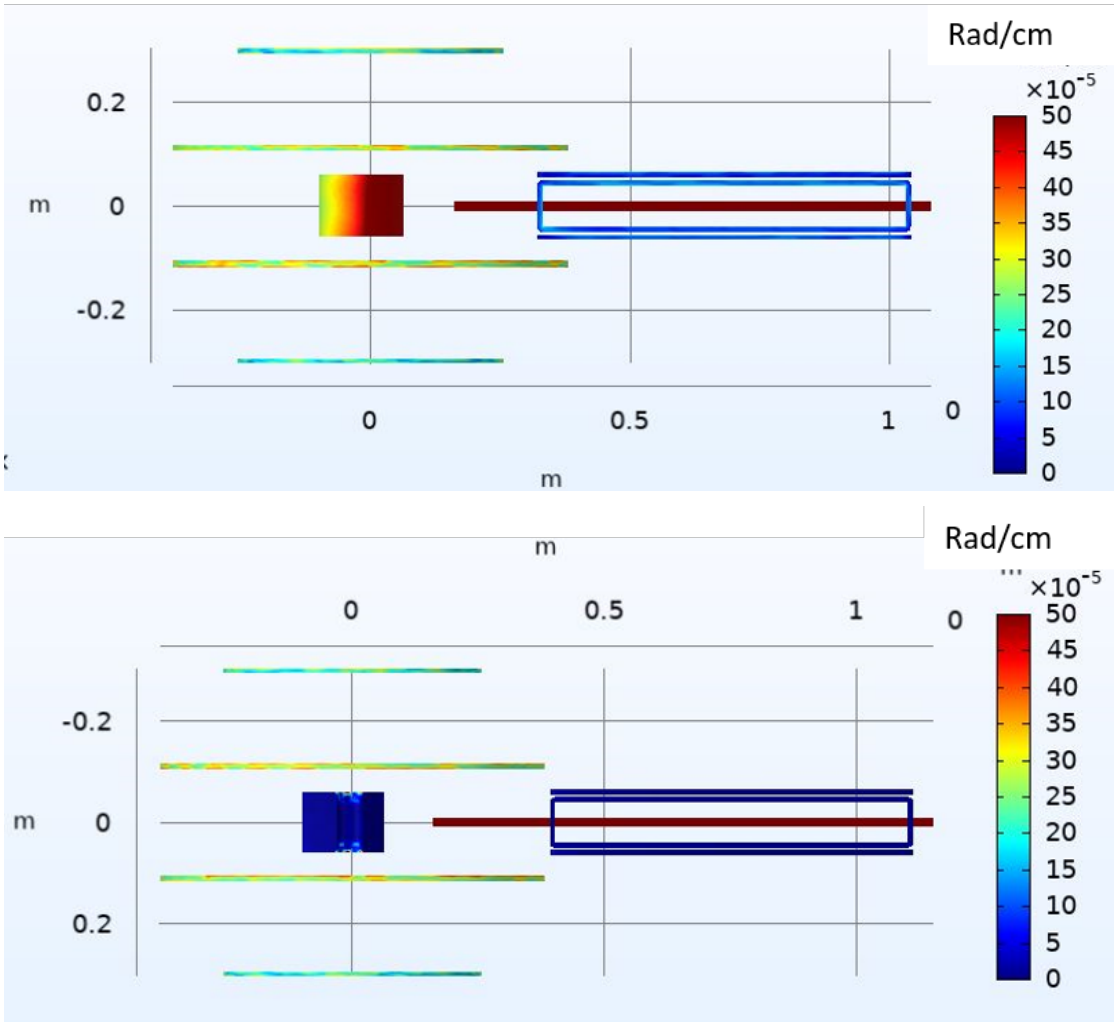

Figure 14: XY view of magnetic field direction angular gradient in the ^{3}He cell for the initial setup. On top for a distance tetracoil-guide field of 33 cm, on the bottom for current only in the tetracoil.

In order to reduce the influence of the guide field on the ^{3}He cell, it was tried to reduce the current or the size of the rectangular coils. The drawback of this approach is that the spin-transport over the whole guiding region becomes worse. After multiple attempts, it was concluded that the only effective solution was to modify the original setup.

One might notice an unexpected computational error at one side of the He cell. This is due to a computational problem in COMSOL, when it is difficult for the mesh to approximate certain shapes. One could verify this by looking at a simulation in which the current in the guide field coils is set to 0 (see the the lower panel of Figure 14). As expected, the magnetic field direction angular gradient gets close to 0, since the field produced by the tetracoil is highly uniform. In order to partially overcome the computation problem, it was necessary to build a particularly fine mesh for the cell itself, as mentioned in section 3.2. However, it was not possible to completely eliminate this problem, since a mesh that is too fine would require too long computation time and can result in non-convergence in the computational process.

4.2.2 Nested coils setup

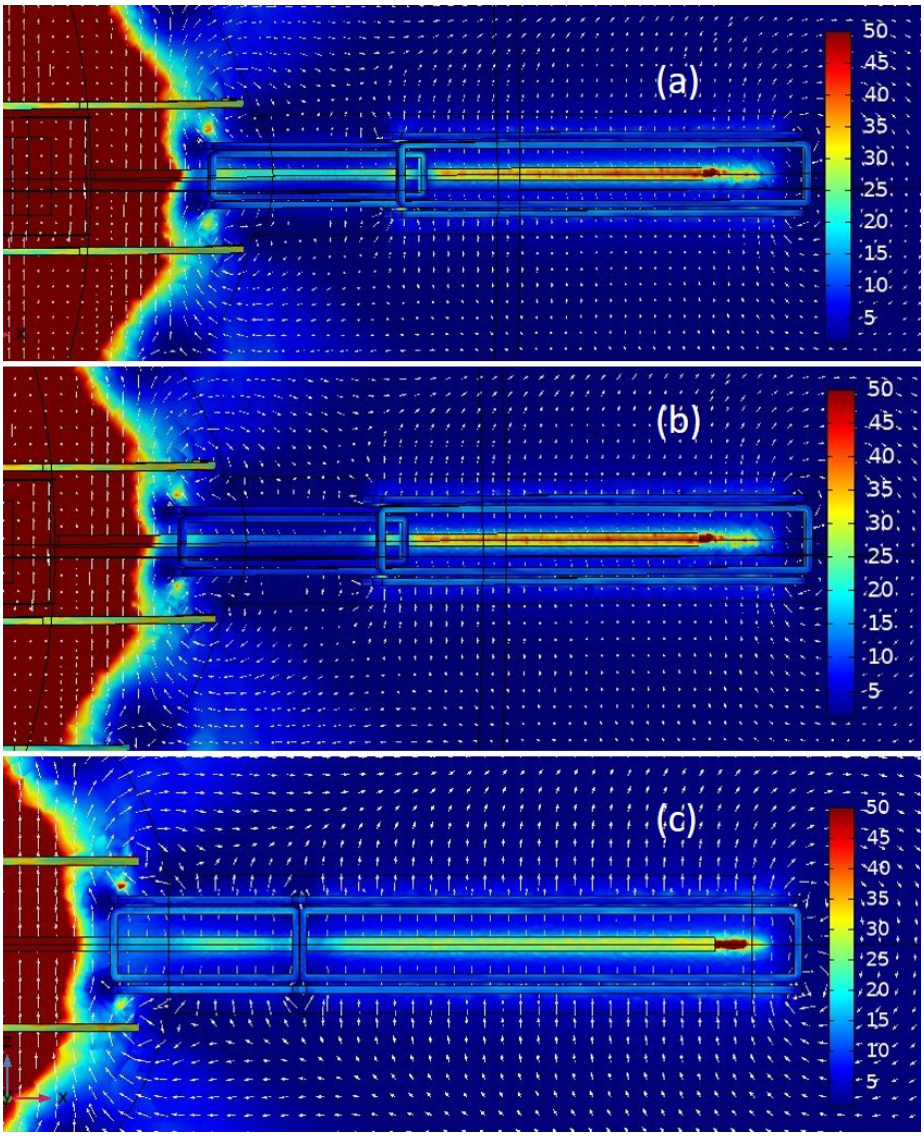

Figure 15: Neutron adiabaticity for the nested setup. The bigger coils were set to a size of 80 mm and a current of 2 A. The distance between the He cell and the guide field coils was set to 35 cm. (a) The smaller guide field coils were set to a size of 55 mm and a current of 1.8 A. (b) The smaller guide field coils with a size of 55 mm and current of 1.2 A. (c) The coils are not nested and the current was set to 2 A and the size to 80 mm for both the coils.

Since it was not possible to achieve both good spin-transport and low magnetic field gradient over the ^{3}He cell with the original setup, it was tested to add four extra coils nested inside the original ones. These extra coils were set to a current of ~90%, and to a size of 68%, compared to the original ones. This was done in order to cover the full flight path of the neutrons without excessively affecting the ^{3}He cell (see Figure 10 (c) and (d)).

As can be seen in Figure 15 (a), this configuration gives better results since the neutron spin-transport is more uniform. The condition $A > 10$ is narrowly met over the full neutron flight path. However, one would desire to improve these results further. In case of a mistake in the fabrication of the coils, the proposed setup would probably fail. In addition, this configuration has one more problem. The magnetic field produced from the inner guide coils disturbs the field produced by the outermost ones. This has as the consequence that the current in the inner coils cannot be much lower than in the outermost ones. Otherwise the transport in the inner coils would deteriorate as shown in Figure 15 (b). In this simulation, the current in the inner coils was set to 60 % of the current in the outer coils. That is why the magnetic field direction angular gradient in the ^{3}He cell shown in Figure 16 did not decrease compared to the initial setup. The reason for designing the coils to be nested instead of parallel was to avoid that the spin-transport would decrease in the junction between the two different rectangular coil structures, as shown in Figure 15 (c).

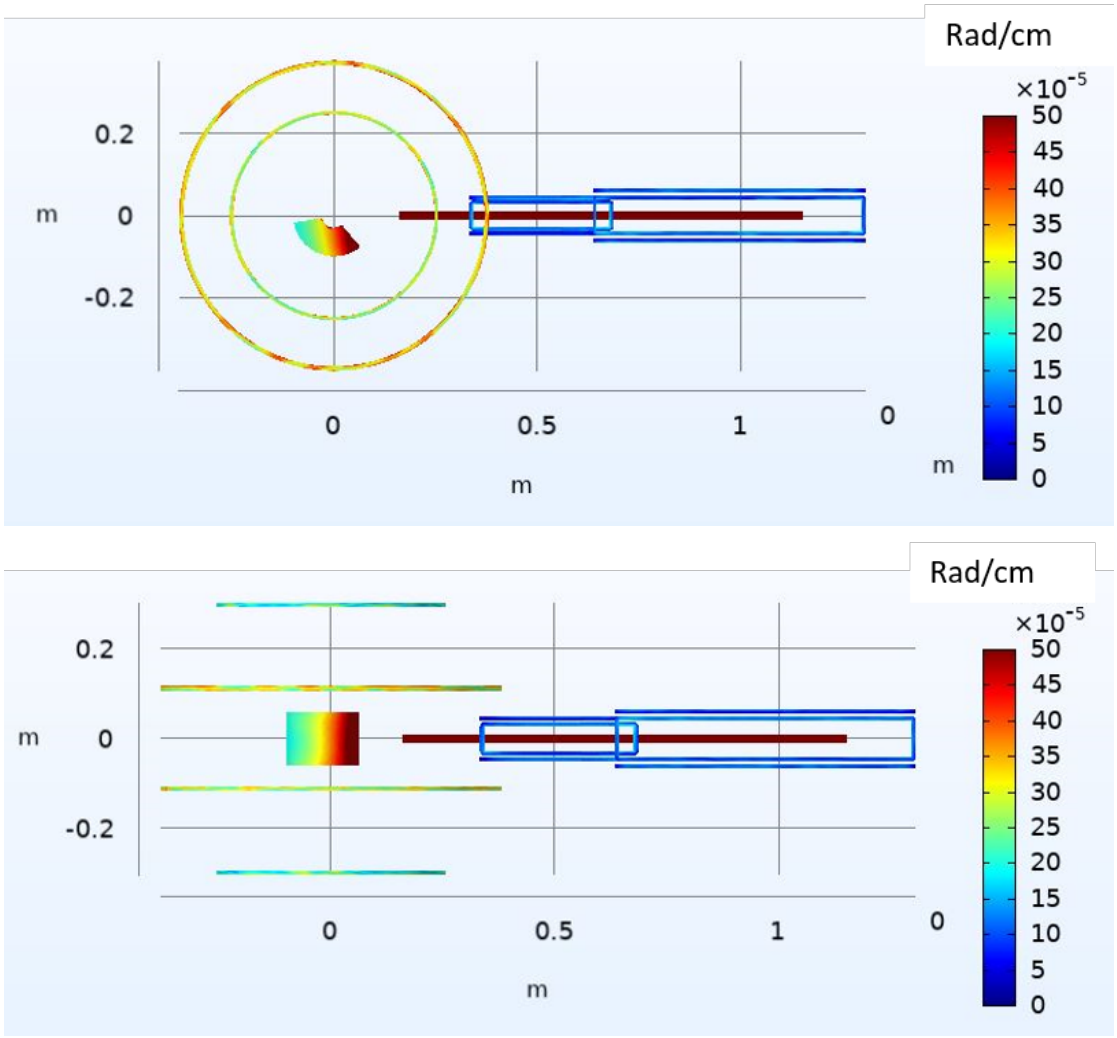

Figure 16: Magnetic field direction angular gradient in the ^{3}He cell for the nested setup. XY view on top and XZ view on the bottom

4.2.3 Halbach four-coil setup

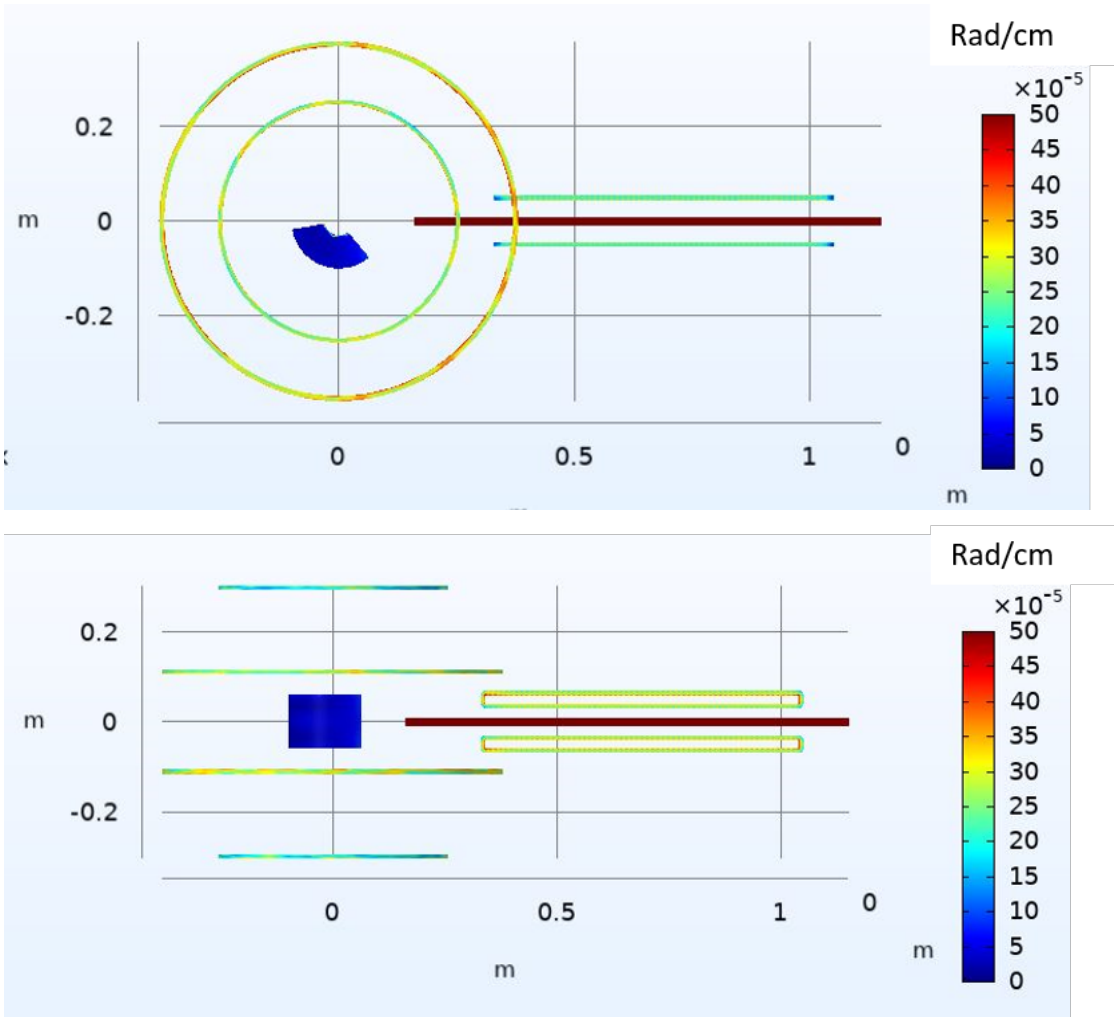

Figure 17: Magnetic field direction angular gradient in the ^{3}He cell for the Halbach setup. XY view on top and XZ view on the bottom.

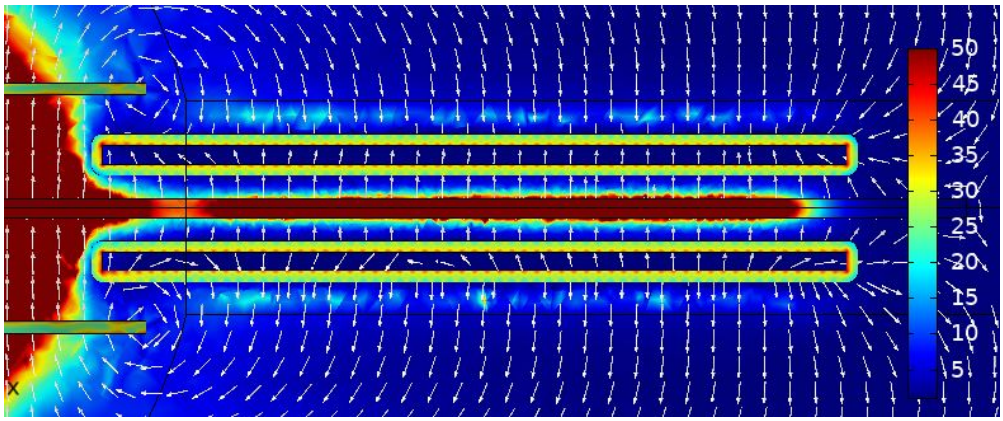

Figure 18: Neutron adiabaticity for the Halbach setup. The Halbach was set to a size of 50 mm and a current of 10 A.

It was concluded that additional adjustments of the setup were needed in order to solve the issues that had been identified with the previous designs. This was accomplished by using a Halbach four-coil (see Figure 10 (e) and (f)). As can be seen in Figure 17 and 18, the neutron spin-transport is excellent over the full flight path ($A > 20$ everywhere) and the magnetic field direction angular gradient is below $1.5 \cdot 10^{-4}$rad/cm over the volume of the ^{3}He cell. The reason for this is the following. As discussed in section 2.5, the Halbach four-coil can be treated as a magnetic quadrupole. While in all the previous setups the structure of the guide field coils can instead be treated as a magnetic dipole. This means that the magnetic field produced by the Halbach four-coil tends to zero more quickly with respect to the distance from the center of the setup. Hence, one can use it to cover the full neutron flight path and increase the current in order to improve the neutron spin-transport without disturbing the magnetic field of the tetracoil.

5 Conclusion and additional work

To summarize, the purpose of this project was the design of the magnetic field for the analyser of the ESS instrument DREAM. This required to optimize neutron spin-filtering and spin-transport and to understand the related theory. In particular, it was necessary to study neutron scattering (nuclear and magnetic), neutron spin-transport in magnetic fields, the finite element method and how to produce uniform magnetic fields with coils. The design of the magnetic field was carried out using the FEM based simulation software COMSOL. After multiple attempts using different setups with rectangular coils, the magnetic field has been successfully designed using a Halbach four-coil system.

In order to improve the results, one could investigate one more setup, which would consist of a Halbach eight-coil system. As mentioned in section 2.6, this structure would behave as a magnetic octupole. For the same reason that the Halbach four-coil gave better results than the first setups, this setup could probably do even better as one could increase the current in the coils even more. Such a setup would, however, be less practical to fabricate. Moreover, it will be necessary to refine the model even further and to make sure that the design fits with the instrument's engineering constraints. The tetracoil provides a uni-directional uniform field. There are applications where a 3-dimensional uniform field will be needed. Additional work will be needed to explore such a field coil assembly that has as little coil material as possible in the path of the scattered neutrons.

References

[1] Comsol multiphysics. https://www.comsol.com/.

[2] Gary J. Russell *et.al.*. Spallation physics - an overview. *ICANS-XI Internationl collaboration on advanced neutron sources, KEK, Tsukuba, October 22-26, 1990*.

[3] Yngve Inntjore Levinsen, M. Eshraqi, R. Miyamoto, M. Munoz., A. Ponton, and R. De Prisco. Beam dynamics challenges in ess linac. *Proceedings of the 57th ICFA Advanced Beam Dynamics Workshop on High-Intensity, High Brightness and High Power Hadron Beams, ISBN 978-3-95450-178-6, p.315 (2016)*.

[4] Pierre M. Lapostolle. Proton linear accelerators: a theoretical and historical introduction. *Report number: LA-11601-MS, Los Alamos, New Mexico, (1989)*.

[5] G. Bacon. Neutron diffraction, 2nd ed., chapters 2.1, 2.2, 2.4. *Oxford: Clarendon Press (1962).*.

[6] G.L. Squires. Introduction to the theory of thermal neutron scattering, section 9.4. *Cambridge University Press (1996)*.

[7] M. Batz *et.al.*. ^{3}he spin filter for neutrons. *J Res Natl Inst Stand Technol. (2005) May-Jun;* ***110*** *(3): 293–298.*.

[8] T.R. Gentile *et.al.*. Polarized spin filters in neutron scattering. *, Physica* ***B 356****, 56 (2005).*.

[9] Malcolm H. Levitt. Spin dynamics. *Wiley (2001)*.

[10] M. Maldonado-Velázquez, L. Barrón-Palos, C. Crawford, and W.M. Snow. Magnetic field devices for neutron spin transport and manipulation in precise neutron spin rotation measurements. *Nucl. Instrum. Methods Phys. Res., A. 854, 127 (2017).*.

[11] G. D. Cates, S. R. Schaefer, and W. Happer. Relaxation of spins due to field inhomogeneities in gaseous samples at low magnetic fields and low pressures. *Phys. Rev.* ***A 37****, 2877 (1988)*.

[12] Miroslav Stanojevic and Miroslav Prsa. Analysis of coil systems for homogeneous magnetic field generation. *12th International Conference on Applied Electromagnetics - MEC (2015)* .

[13] G. Gottardi, P. Mesirca, C. Agostini, D. Remondini, and F. Bersani. A four coil exposure system (tetracoil) producing a highly uniform magnetic field. *Bioelectromagnetics 24:125-133 (2003)*.

[14] R. Merritt, C. Purcell, and G. Stroink. Uniform magnetic fields produced by three, four and five square coils. *Rev. Sci. Instrum* ***54****, 879 (1983)*.

[15] K. Halbach. Design of permanent multipole magnets with oriented rare earth cobalt material. *Nucl. Instrum. Methods.* ***169****, 1 (1980)*.

[16] Solidworks. https://www.solidworks.com/.

[17] Andrew Griesmer. How to use comsol multiphysics, a tutorial video. https://www.comsol.com/blogs/how-to-use-comsol-multiphysics-a-tutorial-video/.